Anisotropy in a stratified shear layer

J. Werne and D. C. Fritts

Colorado Research Associates/NWRA, Boulder, Colorado

Camera-ready Copy for

Physics and Chemistry of the Earth

Manuscript-No. NP3.4-0011

Offset requests to:
J. Werne
Colorado Research Associates/NWRA
Boulder, Colorado

Anisotropy in a stratified shear layer

J. Werne and D. C. Fritts
Colorado Research Associates/NWRA, Boulder, Colorado

Received 19 April 1999 – Accepted 19 April 1999

Abstract. The dynamics and turbulent evolution of a stratified shear layer are explored through direct numerical simulation. Turbulence is instigated through the most unstable asymptotic linear Kelvin-Helmholtz (KH) eigenmode at Richardson number $Ri = 0.05$ and Reynolds number $Re = 2000$ (Ri and Re are defined below). The primary 2D KH vortex succumbs to 3D motions in a manner consistent with earlier findings. The shear-layer Reynolds number Re_L (defined below) grows to $Re_L \approx 2.4 \times 10^4$ as the layer expands and small length-scale motions develop. Large- and small-scale anisotropy are examined by comparing 1) spectra for the longitudinal and transverse correlation coefficients, 2) RMS velocity components and 3) velocity and temperature derivatives during the time when turbulence is most intense. The mean shear produces a tendency toward streamwise axisymmetric, as opposed to isotropic, turbulent flow; however, departures from streamwise axisymmetry due to stratification are evident in the dissipation fields (*i.e.*, at small scales).

1 Introduction

Three-dimensional (3D) turbulence in the atmosphere and ocean results from anisotropic forcing by buoyancy or velocity shear. It is common to assume that the smaller length scales develop isotropy as turbulent kinetic energy cascades in wavenumber space from low to high wavenumbers; however, in recent years concern has mounted over the applicability of isotropic relations to stratified turbulence in the ocean, even at the smallest (*i.e.*, dissipation) length scales (Gregg and Sanford, 1988; Gargett, 1989; Yamazaki and Osborn, 1990; Thoroddsen and Van Atta, 1992). Convincing evidence of small-scale anisotropy resulting when stratification dominates the late-time signature of the flow has been presented, either when $Re_b = \epsilon/\nu N^2$ drops below $Re_b \approx 20$ (Yamazaki and Osborn, 1990), or when stratified turbulence is observed sufficiently far downstream of a turbulence-inducing grid (Thoroddsen and Van Atta, 1992). Here ν, N and $\epsilon = 2\nu s_{ij} s_{ij}$ are the kinematic viscosity, the Brunt-Väisälä frequency, and the kinetic-energy dissipation rate, respectively. $s_{ij} = (\partial_i u_j + \partial_j u_i)/2$ is the stress tensor, and ∂_i represents differentiation in the i-direction. Small-scale anisotropy in the velocity field is gaged by examining the relative magnitudes of the 12 velocity-gradient terms of the form $\partial_i u_j \partial_k u_m$ that comprise ϵ. Because not all of the terms are easily accessible experimentally (typically only 3 or fewer are measured), Thoroddsen and Van Atta (1992) stress that a detailed understanding of the relative magnitudes of all the terms would be useful in interpreting field or laboratory estimates of ϵ based on fewer measurements. In particular, Thoroddsen and Van Atta show that by measuring just three of the dissipation terms, departure from the vertical axisymmetry suggested by Yamazaki and Osborn (1990) for strongly stratified flows is evident. However, as Thoroddsen and Van Atta point out, in order to understand the underlying asymmetries, more velocity-gradient terms must be measured.

In the work reported here, all of the terms needed to compute ϵ are evaluated, and small-scale anisotropy is studied in detail. We concentrate specifically on the time when 3D turbulence is most intense and therefore exhibits its closest approach to isotropy for an evolving shear layer triggered by the KH instability. By examining the time when turbulence intensity peaks and, therefore, stratification effects are weakest, the tendency towards streamwise axisymmetry instigated by the mean shear is more easily observed. The competing effects of shear and stratification as a function of depth through the layer is discussed. In particular, the dominance of stratification in the entrainment zones bounding the shear layer is demonstrated.

Correspondence to: J. Werne

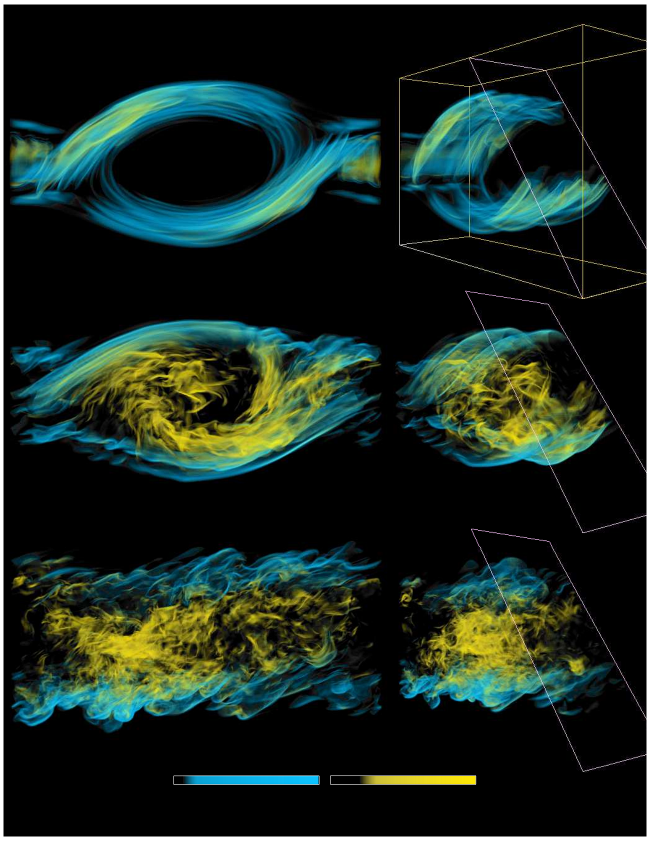

Fig. 1. Viscous (yellow) and thermal (blue) dissipation rates at $t = 66$, 103 and 164, side and perspective views.

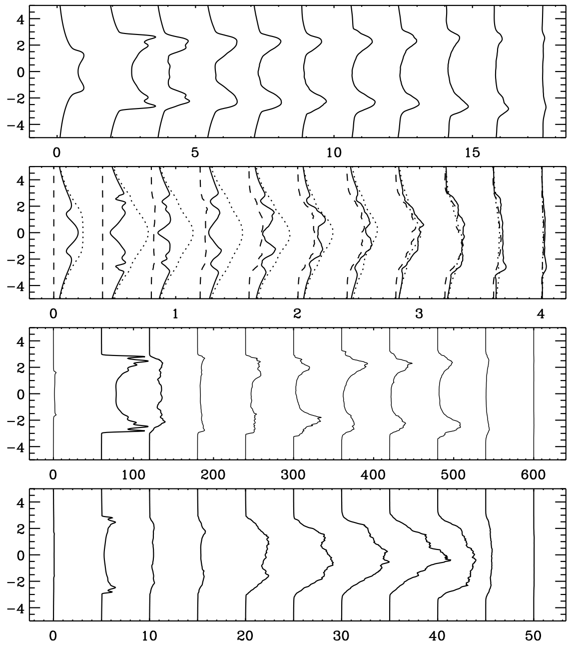

Fig. 2. Profiles with height z for (a) RMS T, (b) RMS u (solid), v (dashed) and w (dotted), (c) χPe and (d) ϵRe at $t = 20$, 49, 66, 83, 103, 117, 134, 142, 165, 220, and 312. Mean profiles are removed from T and u before computing the RMS.

The mathematical formulation of our model is presented in §2. Layer evolution is described in §3. Kinematic relationships for longitudinal and transverse spectra derived for isotropic turbulence are examined in §4. Detailed comparisons of RMS velocity components in §5 and terms comprising the viscous and thermal dissipation fields in §6 reveal information about flow asymmetries at the smallest length scales. Discussion and conclusions appear in §7.

2 Formulation

The basic formulation of the problem includes a Cartesian geometry with a streamwise background flow $u = U_o \tanh(z/h)$, where U_o and h are constant velocity and length scales, and z is the vertical dimension. The background temperature is linear: $T = \beta z$, where β is the mean initial gradient. The Boussinesq (*i.e.*, incompressible) formulation of the equations of motion is used:

$$\partial_t \vec{u} + \vec{\omega} \times \vec{u} = Re^{-1} \nabla^2 \vec{u} - \vec{\nabla} P - Ri\, T \hat{z} \ , \qquad (1)$$

$$\partial_t T + \vec{u} \cdot \vec{\nabla} T = Pe^{-1} \nabla^2 T \ , \text{ and} \qquad (2)$$

$$\vec{\nabla} \cdot \vec{u} = 0 \ . \qquad (3)$$

Eqs. (1)–(3) express momentum, heat, and mass conservation for the system; $\vec{u} = (u, v, w)$ and $\vec{x} = (x, y, z)$ are velocity and position vectors; $\vec{\omega} = \vec{\nabla} \times \vec{u}$ is the vorticity; and T is the temperature. All quantities are non-dimensional, using characteristic time, length, velocity, and temperature scales h/U_o, h, U_o, and βh. $Ri = N^2/\max(\partial_z u)^2$, $Re = U_o h/\nu$, and $Pe = U_o h/\kappa$ are the Richardson, Reynolds, and Peclet numbers. κ is the thermal diffusivity. $Ri = 0.05$ and $Re = Pe = 2000$ are used for the 3D solutions presented below. Equality of Re and Pe implies $Pr = \nu/\kappa = 1$, which is near the value for air ($Pr_{air} \approx 0.7$), while $Ri < 0.25$ indicates dynamic instability for the stratified layer (Miles, 1961).

Boundary conditions are periodic in horizontal directions and stress-free on the top and bottom boundaries. Solutions are obtained with a pseudo-spectral Galerkin algorithm with field variables represented spatially by Fourier series. The hybrid implicit-explicit, 3rd-order Runge-Kutta timestepping suggested by Spalart et al. (1991) is implemented with a CFL criterion of 0.68. A more detailed description of a similar version of the numerical algorithm can be found in Julien et al. (1996).

We initiate motion with the most rapidly growing asymptotic linear eigenmode ($\lambda \approx 4\pi$, but slightly dependent on Re) superposed with a Kolmogorov noise spectrum added to the velocity field. Vorticity amplitudes for these perturbations are 0.07 and 0.014, respectively. To accommodate the eigenmode and the anticipated "secondary instability" (Klaassen and Peltier,

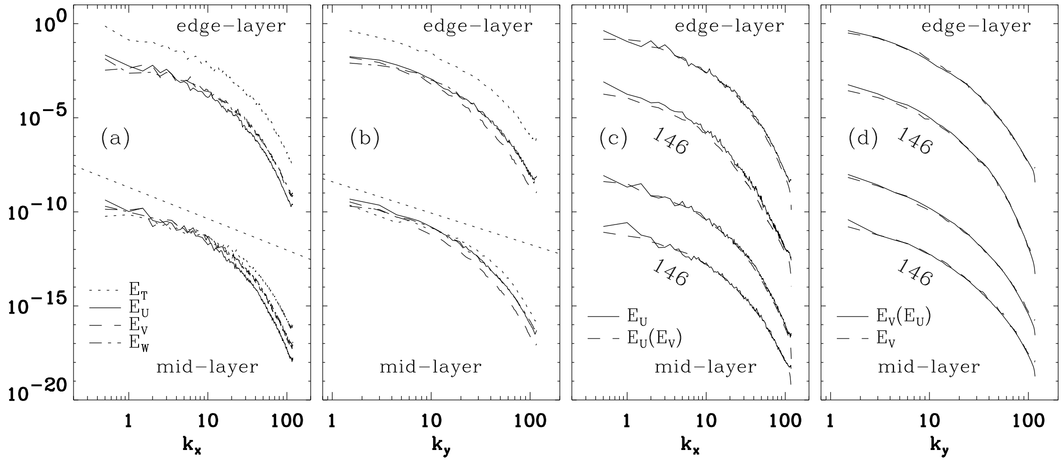

Fig. 3. T, u, v and w spectra versus (a) k_x and (b) k_y at $t = 164$ for $z = 0.0$ and 2.4; $k^{-5/3}$ (dashed) is also shown. Comparison with Eq. 4 for (c) u and (d) v spectra in k_x and k_y at $t = 146$ (labeled) and $t = 164$.

1985, 1991; Palmer et al., 1994), horizontal dimensions of $x_o \times y_o = 12.56 \times 4.2$ are used. Sufficient remoteness of top and bottom boundaries is established with 2D tests, and $z_o = 25$ is chosen.

Spatial resolution is varied during the evolution so that small-scale features are always properly represented. With $Re = 2000$, as many as $720 \times 240 \times 1440$ spectral modes are required. For comparison with naturally occurring shear layers (for which the final full layer depth L is measured, but h is not), the layer Reynolds number $Re_L = \Delta U L/\nu$ based on the velocity difference ΔU across the layer and L is roughly $Re_L \approx 2.4 \times 10^4$. This should be compared to mesospheric (Lübken, 1992), stratospheric (Ierkic et al., 1990), and oceanic (Seim and Gregg, 1994) observations of $Re_L \approx 10^4$, 3×10^6, and 3×10^6, respectively.

3 Evolution

Fig. 1 depicts the dynamics and mixing of the shear layer through the viscous ϵ (yellow) and thermal χ (blue) dissipation rates during the layer evolution. Here $\chi = \partial_i T \partial_i T$. The primary KH vortex (or billow) becomes baroclinically unstable to the formation of streamwise-aligned vortex tubes (Klaassen and Peltier, 1985; Palmer et al., 1994; Schowalter et al., 1994; Palmer et al., 1996). Interactions between these tubes, the primary KH vortex, and the background shear fuels a turbulent cascade to smaller scales (Fritts et al., 1998). Intense mixing is evident in the partitioning of the dissipation fields: while ϵ is most intense at mid-layer, indicating strong turbulence there, χ concentrates at the layer edges where entrainment of ambient fluid and excursions of turbulent well-mixed fluid maintain intense thermal gradients. Homogenization of the thermal field by turbulent motions at mid-layer dramatically reduces thermal gradients there.

Evolution of profiles for RMS quantities and the dissipation fields are shown in Fig. 2. A strong vertical velocity at mid-layer and fluctuations in u and w at the edges of the layer result from the primary vortex roll-up. Fluctuations in the spanwise velocity v appear with 3D instability at $t \approx 50$ and become evident by $t = 66$. Peaks in the RMS temperature field at the layer's edges initially appear as the KH vortex winds fluid of different temperatures, but persist as a result of turbulent entrainment. The partitioning of ϵ and χ emerges with the appearance of intense small-scale turbulence ($t \approx 100$).

4 Spectral Anisotropy

Fig. 3a,b depicts horizontal spectra at mid-layer and in the edge regions of the turbulent layer at time $t = 164$ when turbulent motion in the layer is at its most vigorous. Mid-layer spectra are shifted down in the plot by 10^{-8}. Note, $t = 164$ is the same time as the lower panels in Fig. 1. The $-5/3$ power law (arbitrary normalization) indicates the Kolmogorov prediction for isotropic turbulence. The temperature spectra in the edge regions is enhanced by more than two orders of magnitude, consistent with the more intense thermal fluctuations there (see Fig.s 1 and 2).

Fig. 3c,d tests the isotropy of the spectra. Data for the slightly earlier time $t = 146$ is also included so that some sense of the evolution of anisotropy can be gaged during intense turbulence. The longitudinal spectra $E_u(k_x)$ (in 3c) and $E_v(k_y)$ (in 3d) for $t = 164$ are identical to those in Fig. 3a,b. Predicted isotropic spectra $E_u(E_v)$ and $E_v(E_u)$ are also included; they are obtained from the transverse spectra $E_v(k_x)$ (in 3c) and $E_u(k_y)$ (in 3d)

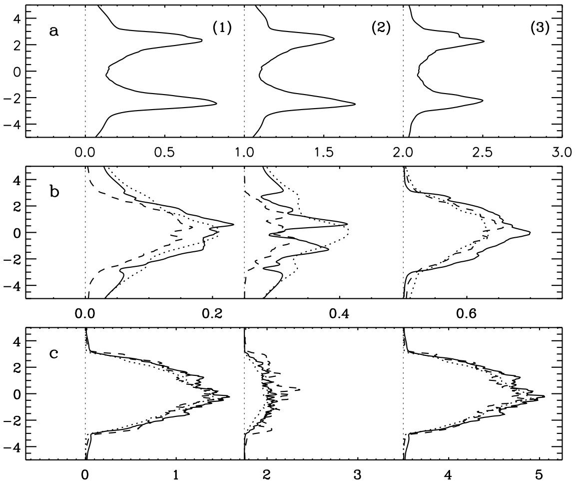

Fig. 4. RMS profiles for (a) T, (b) $\vec{v}$, and (c) $\vec{\omega}$ at $t = 146$. The full RMS is plotted in column (1). Spanwise-averaged quantities $\tilde{T}$, $\tilde{\vec{v}}$, and $\tilde{\vec{\omega}}$ are included in column (2), and fluctuation quantities T', $\vec{v}'$, and $\vec{\omega}'$ are included in column (3). Streamwise, spanwise and vertical components are shown with solid, dashed and dotted linestyles, respectively.

and the isotropic relation

$$E_1(k_x) = 2k_x \int_{k_x}^{\infty} \frac{E_2(k)}{k^2}\, dk \ , \tag{4}$$

which we deduce upon integrating the better-known form (Hinze, 1959)

$$-2E_2(k_x) = k_x\ \partial_{k_x} E_1(k_x) - E_1(k_x) \ . \tag{5}$$

The figure indicates isotropy to be a good approximation at mid-layer; however, the reader should be warned, comparisons on log-log scales are not critical, and examination of the same spectra on a linear-log scale (not shown) reveals departures from isotropy from 10% to 80%, depending on the wavenumber. At the earlier time $t = 146$ the spectra in the edge regions are more notably anisotropic, exhibiting deviations of 200% to 300%.

5 RMS Anisotropy

The large-scale anisotropy in the shear layer at $t = 146$ is evident in the RMS profiles for u, v, and w; see Fig. 4. Interpretation of the profiles is simplified by the decomposition $\psi = \bar{\psi} + \tilde{\psi} + \psi'$ (Fritts et al., 1996) where ψ represents a flow field, *e.g.*, T, u, *etc.* ((1) in Fig. 4), $\bar{\psi}$ is the horizontal average of ψ, $\tilde{\psi}$ is the spanwise average of $\psi - \bar{\psi}$ ((2) in Fig. 4), and ψ' is the balance ((3) in Fig. 4). Following Fritts et al. (1996) we associate $\tilde{\psi}$ at mid-layer with 2D billow and $\bar{\psi}$ with the background mean. ψ' is the small-scale 3D fluctuations. With flow fields decomposed in this way, a clear (though weak) 2D billow signature is apparent in the spanwise averages of u, v, and w, as is evident when compared to earlier times when the billow signature is much stronger (see Fig. 2).

At mid-layer ($z = 0$), the RMS fluctuations u', v', and w' depict a near axisymmetric character (with $v' \approx w'$ and $u\prime > v\prime$). The mean shear establishes x as the unique direction in the flow, even at the smallest length scales. Note however that Fig. 4 also reveals a slight suppression of w' relative to v' due to buoyancy. Admittedly, this effect is barely evident in Fig. 4, but it will be demonstrated more convincingly with velocity gradients below.

Near the edges of the shear layer, the relative magnitudes of u', v', and w' differ from the near streamwise axisymmetric ratios at mid-layer. The character of the flow is indicated by profiles of RMS vorticity (Fig. 4c) which show enhanced streamwise vorticity throughout the layer, resulting from stretching by the mean shear. At the outer-most reaches of the turbulent layer, spanwise vorticity is elevated above the other two components as a result of the increased stratification (relative to the background shear) at the layer's edges (*e.g.*, see profiles of $Ri(z)$ in Werne and Fritts (1999)).

6 Dissipation anisotropy

For homogeneous, isotropic turbulence, the following relations apply (Monin and Yaglom, 1975):

$$\langle \partial_x u \partial_x u \rangle = \langle \partial_y v \partial_y v \rangle \ , \ \langle \partial_x v \partial_x v \rangle = 2 \langle \partial_x u \partial_x u \rangle$$
$$\text{and } \langle \partial_x v \partial_y u \rangle = -\frac{1}{2} \langle \partial_x u \partial_x u \rangle \ . \tag{6}$$

Similar equations relating other longitudinal, transverse, and cross terms can also be derived, and all thermal dissipation terms are equal; *e.g.*, $\langle \partial_x T \partial_x T \rangle = \langle \partial_y T \partial_y T \rangle$. Fig. 5 demonstrates that these symmetry constraints are too severe for our turbulent shear layer: the left-most profile shown in Fig. 5a overlays all of the velocity-derivative terms (multiplied by 1, 2, or -0.5, as appropriate according to Eq. 6), and significant departures from equality are evident in the range of the results.

As was noted in §5, the anisotropy at small scales demonstrated by Fig. 5a,d (left-most curves) is anticipated already from curves (3) in Fig. 4b. In fact, from the results presented in §5, we expect better agreement with streamwise axisymmetry rather than isotropy, for which different relationships among the velocity gradients hold (George and Hussein, 1991):

$$\langle \partial_y v \partial_y v \rangle - \langle \partial_x u \partial_x u \rangle = \langle \partial_z w \partial_z w \rangle - \langle \partial_x u \partial_x u \rangle =$$
$$\langle \partial_y u \partial_x v \rangle - \langle \partial_z v \partial_y w \rangle = \langle \partial_z u \partial_x w \rangle - \langle \partial_z v \partial_y w \rangle \tag{7}$$

$$\langle \partial_y u \partial_x v \rangle = \langle \partial_z u \partial_x w \rangle \ , \ \langle \partial_y u \partial_y u \rangle = \langle \partial_z u \partial_z u \rangle$$
$$\langle \partial_x v \partial_x v \rangle = \langle \partial_x w \partial_x w \rangle \ , \ \langle \partial_z v \partial_z v \rangle = \langle \partial_y w \partial_y w \rangle \tag{8}$$

$$\langle \partial_z T \partial_z T \rangle = \langle \partial_y T \partial_y T \rangle \ . \tag{9}$$

Fig. 5b,e shows the four profiles in Eq. 7. Note that the differences in Eq. 7 measure the degree of anisotropy,

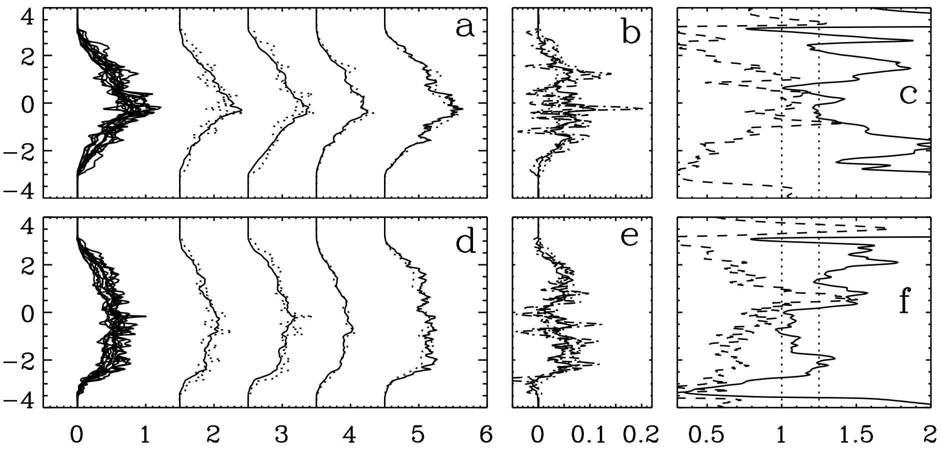

Fig. 5. Profiles with height of horizontally averaged dissipation terms test isotropic and axisymmetric relationships for $t = 146$ (a,b,c) and $t = 164$ (d,e,f). (a,d) Left most curve shows all velocity-derivative correlations appearing in the definition of ϵ (see text). Transverse (cross) terms are multiplied by 0.5 (-2); all curves should overlay for perfect isotropy. The remaining four profile pairs in (a,d) to the right test axisymmetry relations (Eq. 8). They are plotted in the order in which the equations appear in Eq. 8; solid curves represent the terms to the left of the equals sign. $\langle\partial_z u \partial_z u\rangle$ and $\langle\partial_x w \partial_x w\rangle$ are multiplied by 1/1.16 (1/1.06) and 1.16 (1.06), respectively, for $t = 146$ ($t = 164$) to reveal the degree to which axisymmetry is violated by buoyancy effects; similarly, $\langle\partial_y w \partial_y w\rangle$ is multiplied by 1.35 (1.12). (b,e) All curves in Eq. 7 are included; no multiplication factors are applied. (c,f) χ_y/χ_x (solid) and χ_y/χ_z (dashed) versus height. Values of 1.0 and 1.25 are indicated (dotted); see text for definitions.

since zero values are obtained in the isotropic limit. Also note that the agreement in Fig. 5b,e is actually much better than in the left-most curves of Fig. 5a,d; *i.e.*, curves in 5b,e range over typically 0.1, while those in the left-most plot of 5a span roughly 0.6; hence, streamwise axisymmetric turbulence seems a better description of the flow than isotropic turbulence.

The remaining four right-most curves in Fig. 5a,d probe Eq. 8. While the first relation in Eq. 8 appears satisfactory, the second and third exhibit departures of 16% (6%), and the fourth reveals departures of 35% (12%) at $t = 146$ ($t = 164$). These discrepancies are hidden in the plots by reducing $\langle\partial_z u \partial_z u\rangle$ by the factor 1/1.16 (1/1.06), by compensating $\langle\partial_x w \partial_x w\rangle$ by 1.16 (1.06), and by increasing $\langle\partial_y w \partial_y w\rangle$ by 1.35 (1.12) relative to $\langle\partial_z v \partial_z v\rangle$.

Such departures from axisymmetry are expected if stable stratification is significant: suppression of w relative to u and v and of typical vertical length scales δ_z relative to horizontal scales δ_H is anticipated if buoyancy influences the motion (Riley et al., 1981; Lilly, 1983). If all occurrences of w in Eqs. 7–9 are reduced by ≈ 1.077 (≈ 1.03) and those including ∂_z are increased by 1.077 (1.03), the behavior in Fig. 5a,b is predicted for $t = 146$ ($t = 164$). Note that this simple characterization of the effects of buoyancy appears better for the earlier time $t = 146$ where the right four pairs of curves in Fig. 5a agree through the full depth of the turbulent layer. For $t = 164$, the correction of 1.03 brings the center portion of the layer into agreement for all of the curves, while near the edges discrepancies persist. Also note that Fig. 5b,e reveals uniform departures of isotropy throughout most of the layer at $t = 146$, while a tendency towards isotropy in the center of the layer is revealed at $t = 164$. Near the edges anisotropy persists.

Fig. 5c,f shows the ratios χ_y/χ_z (dashed) and χ_y/χ_x (solid), where $\chi_i = \langle\partial_i T \partial_i T\rangle$. Departure from isotropy at mid-layer is difficult to discern, given the fluctuations in χ_y/χ_z and χ_y/χ_x; however, $\chi_y/\chi_z < 1$ is clearly evident at the edges of the layer ($z \approx \pm 3$), demonstrating the reduction of δ_z due to buoyancy. Hence, stratification is greater near the edges of the turbulent layer. The increase in χ_y/χ_x near both of the layer's edges at $t = 146$ reflects the relatively intense streamwise-aligned vortex tubes there which enhance (reduce) spanwise (streamwise) gradients for T; see Fig. 4.

7 Discussion

As a first step to quantifying the anisotropy occurring in a turbulent stratified shear layer, we have examined spectra, RMS velocity components, and the velocity- and temperature-gradient terms that comprise ϵ and χ. By focusing on times during which turbulence is most active, we have demonstrated a tendency toward streamwise axisymmetry resulting from the mean shear. Hence, our results indicate two orthogonal preferred directions (vertical for stratification and streamwise for the mean flow) compete to establish the symmetry properties of the turbulence. We suggest this is the reason for the departure from vertical axisymmetry observed by Thoroddsen and Van Atta (1992). In support of this suggestion, we present the following measurements from our solutions at mid-layer and $t = 146$ and 164: $\langle v'v'\rangle / \langle u'u'\rangle \approx 0.65$, $\langle w'w'\rangle / \langle u'u'\rangle \approx 0.58$, and $Fr^{-1} \approx 1.8$, where $Fr = 3\epsilon/(\langle u_i' u_i'\rangle \sqrt{Ri\, \partial_z \overline{T}})$ is the internal Froude number. These results are consistent with the measurements of Thoroddsen and Van Atta (1992), indicating the tendency to streamwise axisymmetry we observe may also be present in the experiments. We note, however, that mid-layer values for $\langle \partial_x v \partial_x v\rangle / \langle \partial_x u \partial_x u\rangle$ and $\langle \partial_x w \partial_x w\rangle / \langle \partial_x u \partial_x u\rangle$ of ≈ 2 and 1.8, respectively, are higher than observed for Thoroddsen and Van Atta's experiments, indicating a difference between shear and grid-generated turbulence. Nevertheless, we also observe a tendency for $\langle \partial_x v \partial_x v\rangle / \langle \partial_x u \partial_x u\rangle$ and $\langle \partial_x w \partial_x w\rangle / \langle \partial_x u \partial_x u\rangle$ to decrease near the edges of the shear layer (≈ 1 and 1.2, respectively) where stratification is stronger, in qualitative agreement with the grid-turbulence results. Future work will focus on the time evolution of small-scale anisotropy and the evolving competition between shear- and stratification-axisymmetry effects.

In closing, we would like to stress the partitioning of ϵ and χ depicted in Fig. 1. This is a general feature of all turbulent flows confined by stratification and for which entrainment of fluid outside the turbulent layer must occur. Furthermore, as both the index of refraction and the acoustic cross-section are related to the temperature, the basic morphology of χ and ϵ has important implications for radar measurements in the atmosphere (Hocking and Röttger, 1997; Lübken, 1992; Blix et al., 1990a,b; Ierkic et al., 1990; Hocking, 1985) and acoustic backscatter measurements in the ocean (Seim and Gregg, 1994; Seim et al., 1995). Most importantly, the edge regions bounding stratified shear layers exhibit 1) the largest backscatter returns as scalar fields are imperfectly mixed and therefore large scalar gradients persist, 2) the highest degree of anisotropy and 3) coherent motion, rather than turbulence, as stratification overwhelms the shear and effectively lowers the Reynolds number. As a result, the employment of isotropic theory to interpret radar and acoustic backscatter of stratified turbulence should be viewed with suspicion.

Acknowledgements. This work was supported by AFOSR F49620-98-C-0029, DOE DE-FG03-99ER62839, NSF ATM-9708633 and ATM-9816160. Calculations were conducted on the 512-PE Cray T3E at ERDC, with additional resources at PSC and NCSA.

References

Blix, T.A., Thrane, E.V., and Andreassen, Ø., In-situ measurements of the fine-scale structure and turbulence in the mesosphere and lower thermosphere by means of electrostatic positive ion probes, *J. Geophys. Res.*, *95*, 5533-5548, 1990.

Blix, T.A., Thrane, E.V., Fritts, D.C., von Zahn, U., Lübken, F.-J., Hillert, W., Blood, S.P., Mitchell, J.D., Kokin, G.A. and Pakhomov, S.V., Small-scale structure observed *in-situ* during MAC/EPSILON, *J. Atmos. Terr. Phys.*, *52*, 835-854, 1990.

Fritts, D.C., Palmer, T.L., Andreassen, Ø., and Lie, I., Evolution and breakdown of Kelvin-Helmholtz billows in stratified compressible flows, I: Comparision of two- and three-dimensional flows, *J. Atmos. Sci.*, *53*, 3173-3191, 1996.

Fritts, D.C., Arendt, S., and Andreassen, Ø., Vorticity dynamics in a breaking internal gravity wave, 2. Vortex interactions and transition to turbulence, *J. Fluid Mech.*, *367*, 47-65, 1998.

Gargett, A.E., Ocean turbulence, *Annu. Rev. Fluid Mech.*, *21*, 419-451, 1989.

George, W.K., and Hussein, J.H., Locally axisymmetric turbulence, *J. Fluid Mech.*, *233*, 1-23, 1991.

Gregg, M.C., and Sanford, T.B., The dependence of turbulent dissipation on stratification in a diffusively stable thermocline, *J. Geophys. Res.*, *93*, 12,381-12392, 1988.

Hinze, J. O., Turbulence, McGraw-Hill, New York, 1959.

Hocking, W.K., Measurement of turbulent energy dissipation rates in the middle atmosphere by radar techniques, *Radio Sci.*, *20*, 1403-1422, 1985.

Hocking, W.K., and Röttger, J., Studies of polar mesosphere summer echoes over EISCAT using calibrated signal strengths and statistical parameters, *Radio Sci.*, *32*, 1425-1444, 1997.

Ierkic, H.M., Woodman, R.F., and Perillat, P., Ultrahigh vertical reoslution radar measurements in the lower stratosphere at Arecibo, *Radio Sci.*, *25*, 941-952, 1990.

Julien, K., Legg, S., McWilliams J., and Werne, J., Rapidly rotating turbulent Rayleigh-Bénard convection, *J. Fluid Mech.*, *322*, 243-273, 1996.

Klaassen, G.P., and Peltier, W.R., The onset of turbulence in finite-amplitude Kelvin-Helmholtz billows, *J. Fluid Mech.*, *155*, 1-35, 1985.

Klaassen, G.P., and Peltier, W.R., The influence of stratification on secondary instability in free shear layers, *J. Fluid Mech.*, *227*, 71-106, 1991.

Lilly, D.K., *J. Atmos. Sci.*, *40*, 749.

Lübken, F.J., On the extraction of turbulent parameters from atmospheric density fluctuations, *J. Geophys. Res.*, *97*, 20385-20395, 1992.

Miles, J.W., On the stability of heterogeneous shear flows, *J. Fluid Mech.*, *10*, 496-508, 1961.

Monin, A.S., and Yaglom, A.M., Statistical Fluid Mechanics, The MIT Press, Cambridge, 1975.

Palmer, T.L., Fritts, D.C., Andreassen, Ø., and Lie, I., Three-dimensional evolution of Kelvin-Helmholtz billows in stratified compressible flow, *Geophys. Res. Lett.*, *21*, 2287-2290, 1994.

Palmer, T.L., Fritts, D.C., and Andreassen, Ø., Evolution and breakdown of Kelvin-Helmholtz billows in stratified compressible flows, II: Instability structure, evolution and energetics, *J. Atmos. Sci.*, *53*, 3192-3212, 1996.

Riley, J.J., Metcalfe, R.W., and Weissman, M.A., Direct numerical simulations of homogeneous turbulence in density-stratified fluids, in *Proceedings AIP Conference on Nonlinear Properties of Internal Waves*, B. J. West, ed. 79, 1981.

Schowalter, D.G., Van Atta, C.W., and Lasheras, J.C., A study of streamwise vortex structures in a stratified shear layer, *J. Fluid Mech.*, *281*, 247-291, 1994.

Seim, H.E., and Gregg, M.C., Detailed observations of a naturally occuring shear instability, *J. Geophys. Res.*, *99*, 10049-10073, 1994.

Seim, H.E., Gregg, M.C., and Miyamoto, T., Acoustic backscatter from turbulent microstructure, *J. Atmos. Ocean Tech.*, *12*, 367-380, 1995.

Spalart, P.R., Moser, R.D., and Rogers, M.M., Spectral methods for the Navier-Stokes equations with one infinite and two periodic directions, *J. Comput. Phys.*, *96*, 297-324, 1991.

Thoroddsen, S.T., and Van Atta, C.W., The Influence of Stable Stratification on Small-Scale Anisotropy and Dissipation in Turbulence, *J. Geophys. Res.*, *97*, 3647-3658, 1992.

Werne, J., and Fritts, D.C., Stratified shear turbulence: Evolution and statistics, *Geophys. Res. Lett.*, *26*, 439-442, 1999.

Yamazaki, H. and Osborn, T., Dissipation estimates for stratified turbulence, *J. Geophys. Res.*, *95*, 9739-9744, 1990.